T.C.

GEBZE TECHNICAL UNIVERSITY

GRADUATE SCHOOL OF NATURAL AND APPLIED SCIENCE

SURFACE STUDY OF $TlGaSe_2$ AND $TlInS_2$ LAYERED CRYSTALS

EMIR SUAD OLCAY

A THESIS SUBMITTED FOR THE DEGREE OF

MASTER OF SCIENCE

DEPARTMENT OF PHYSICS

GEBZE

2017

T.C.

GEBZE TECHNICAL UNIVERSITY

GRADUATE SCHOOL OF NATURAL AND APPLIED SCIENCES

SURFACE STUDY OF $TlGaSe_2$ AND $TlInS_2$ LAYERED CRYSTALS

EMIR SUAD OLCAY

A THESIS SUBMITTED FOR THE DEGREE OF

MASTER OF SCIENCE

DEPARTMENT OF PHYSICS

THESIS SUPERVISOR

PROF. DR. RAUF SULEYMANLI

GEBZE

2017

T.C.
GEBZE TEKNİK ÜNİVERSİTESİ
FEN BİLİMLERİ ENSTİTÜSÜ

KATMANLI $TlGaSe_2$ VE $TlInS_2$ KRİSTALLERİNİN YÜZEY İNCELEMESİ

EMİR SUAD OLCAY
YÜKSEK LİSANS TEZİ
FİZİK ANABİLİM DALI

DANIŞMANI
PROF. DR. RAUF SULEYMANLI

GEBZE
2017

GEBZE TEKNİK ÜNİVERSİTESİ	**YÜKSEK LİSANS JÜRİ ONAY FORMU**

GTÜ Fen Bilimleri Enstitüsü Yönetim Kurulu'nun 18/01/2017 tarih ve 2017/04 sayılı kararıyla oluşturulan jüri tarafından 06/02/2017 tarihinde tez savunma sınavı yapılan Emir Suad OLCAY'ın tez çalışması Fizik Anabilim Dalında YÜKSEK LİSANS tezi olarak kabul edilmiştir.

JÜRİ

ÜYE
(TEZ DANIŞMANI) : Prof. Dr. Rauf Süleymanlı

ÜYE :Prof. Dr. Mirhasan Seyitsoy

ÜYE :Doç. Dr. Kemal Özdoğan

ONAY

Gebze Teknik Üniversitesi Fen Bilimleri Enstitüsü Yönetim Kurulu'nun
...../...../..... tarih ve ...../..... sayılı kararı.

İMZA/MÜHÜR

SUMMARY

In this thesis, surface properties of $TlGaSe_2$ and $TlInS_2$ crystals were studied to understand the physical model of such crystals under the effect of an external electric field using X-Ray Reflection (XRR), X-ray Diffraction (XRD) and Atomic Force Microscopy (AFM) methods.

Key Words: $TlGaSe_2$, $TlInS_2$, Layered Semiconductors.

ÖZET

Bu tez çalışmasında, $TlGaSe_2$ ve $TlInS_2$ kristallerinin dış elektrik alan altında oluşan mekanizmalarının anlaşılması için X-Ray Yansıma (XRR), X-ray Kırınım (XRD) ve Atomik Kuvvet Mikroskop'u (AFM) metodlarıya çalışmalası yapıldı.

Anahtar Kelimeler: $TlGaSe_2$, $TlInS_2$, Katmanlı Yarıiletkenler.

ACKNOWLEDGEMENTS

First, I would like to thank to my dear friends and collegues, Serdar Gören and Dr.Yasin Şale for their helps and supports.

I also want to say thanks to my mother Nilüfer Gülden Olcay and my father Utku Olcay for giving me their support in everything I wanted to realize and bringing me perspective.

Finally, I would like to thank to my supervisor Prof. Dr. Rauf Süleymanlı for endearing physics to me again by answering every question I asked with patience and for his great guidance for the last few years. Without him I wouldn’t be where I am.

TABLE OF CONTENTS

	Page
SUMMARY	v
ÖZET	vi
ACKNOWLEDGEMENTS	vii
TABLE of CONTENTS	viii
LIST of ABBREVIATONS and ACRONYMS	ix
LIST of FIGURES	xi
LIST of TABLES	xii
1. INTRODUCTION	1
2. $TlGaSe_2$ and $TlInS_2$ CRYSTALS	2
3. EXPERIMENTAL DETAILS	4
4. RESULTS and THEORY	6
4.1. XRD Theory	6
4.2. Bragg Interpretation of The Laue Condition	6
4.3. XRD Resuts	9
4.4. XRR Theory	13
4.4.1. Debye Equation	14
4.4.2. Correlation Function	15
4.4.3. Scattering in Born Approximation	15
4.4.4. Porod's Law	17
4.4.5. Guinier's Law	18
4.5. XRR Results	20
4.6. AFM	26
5. CONCLUSIONS	28
REFERENCES	29
BIOGRAPHY	31

LIST of ABBREVIATIONS and ACRONYMS

Abbreviations And Acronyms		**Explanations**
θ	:	Reflection angle with the planes parallel to surface
2θ	:	Reflection angle with the incident beam
λ	:	Wavelength of incident beam
θ_c	:	Critical angle
Å	:	Ångström
µm	:	Micrometer
σ	:	Cross section
Ω	:	Angular span of detector
b	:	Thompson scattering lenght
c	:	Speed of light
c_i	:	Stoichiometric contribution
Cu	:	Copper
d	:	Interplanar distance
DC	:	Direct Current
deg	:	Degree
div	:	Division
e	:	Electron charge
EF	:	Electric field
eV	:	Electron volts
Ga	:	Gallium
Hz	:	Hertz
I (q)	:	Intensity as a function of scattering vector
I_0	:	Intensity of the incident beam
q	:	Wavenumber
k	:	Wavevector
m_e	:	Electron mass
m_i	:	Molar mass
Na	:	Avagadro constant
N	:	Number density of scattering particles

n	:	Number of layer reflection occurs
nm	:	Nanometer
r_0	:	Electron density
R_g	:	Radius of gyration of scattering objects
S	:	Sulfur
S	:	Surface
Se	:	Selenium
Tl	:	Thallium
$TlGaSe_2$	:	Thallium Gallium diSelenide
$TlInS_2$	:	Thallium Indium diSulfide
AFM	:	Atomic Force Microscope
XRD	:	X-Ray Diffraction
XRR	:	X-Ray Reflection

LIST OF FIGURES

Figure No:		Page
2.1:	Crystal lattice of $TlGaSe_2$.	2
2.2:	Bridgman–Stockbarger method.	3
3.1:	Tektronix PS 280 DC Power Supply.	4
3.2:	Rigaku Smartlab X-Ray Diffractometer.	4
3.3:	Nanoscope multimode AFM.	5
4.1:	Bragg interpretation of constructive and destructive scattering conditions.	8
4.2:	$TlGaSe_2$ B Crystal under no electric field and under 60V.	9
4.3:	$TlGaSe_2$ B Crystal shifting of first peak.	10
4.4:	$TlGaSe_2$ A Crystal under -60V and +30V.	10
4.5:	$TlGaSe_2$ A Crystal shifting of first peak.	11
4.6:	$TlGaSe_2$ F Crystal.	12
4.7:	$TlInS_2$ and $TlGaSe_2$ Crystal.	20
4.8:	$TlInS_2$ Crystal.	21
4.9:	$TlGaSe_2$ B Crystal.	22
4.10:	$TlGaSe_2$ B Crystal Reflectivity as a function of time.	23
4.11:	$TlGaSe_2$ B Crystal Reflectivity at No EF and +60V.	23
4.12:	$TlGaSe_2$ B1 Crystal Guinier and Porod fitting.	24
4.13:	Construction of scattering vector.	24
4.14:	: $TlGaSe_2$ B Crystal AFM Images. a) without electric field, b) after application +30V for 30 mins.	26

LIST OF TABLES

Figure No:		**Page**
4.1:	Used properties in density fit calculations.	21
4.2:	Results of density calculations.	21
4.3:	Digital Instruments NanoScope Device Specifications.	27

1. INTRODUCTION

The main reason semiconductors are highly used in modern electronics is their sensitivity to external factors. Improving the sensing performance by increasing the impurities or changing the structure is not preferred [1].

In layered semiconductors like $TlGaSe_2$ and $TlInS_2$ application of an electric field causes a long-term change in surface properties and becomes a functional way of calibration [2].

In this study, we aim to explain the effect of an externally applied electric field to have a better comprehension of previous works where the electric field alters electronic transport, rectification and memristive behavior, excitonic photoconductivity, and photo response [3-5].

Surface is essential in our study due to its interface nature. An interface can be described as a small number of atomic layers at which the properties change dramatically and the surface is a particular interface where the solid interfere with the atmosphere. Basically, we will be inspecting structural changes caused by the applied electric field within the solid with X-Ray Diffraction (XRD) method and surface changes with X-Ray Reflection (XRR) and Atomic Force Microscopy (AFM) methods.

2. $TlGaSe_2$ AND $TlInS_2$ CRYSTALS

Ternary thallium based chalcogenide semiconductors has the general chemical formula $Tl(AB_2)$ where A can be replaced with In, Ga and B with Se, S. $TlGaSe_2$ and $TlInS_2$ are the most studied thallium based chalcogenides over the last 30 years. In room temperature, they are both monoclinic and belong to C_{2h}^6 space group symmetry and they are both native p-type semiconductors with energy band gap ~2.1-2.2 eV.

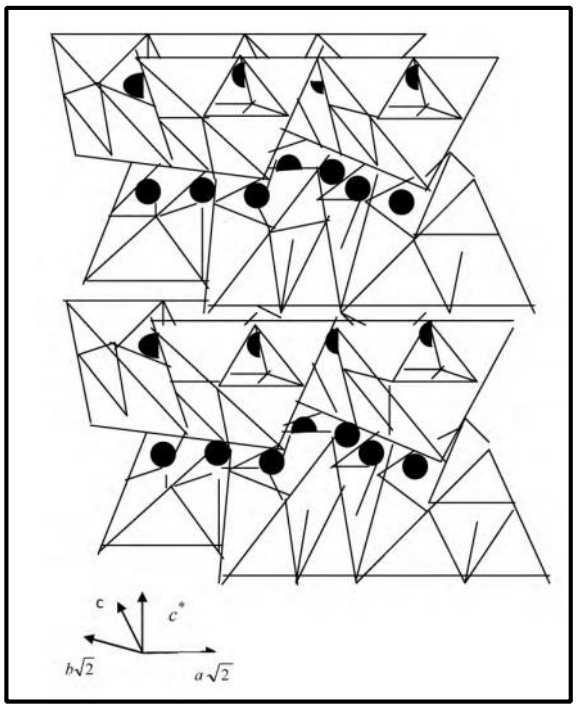

Figure 2.1: An image of crystal lattice of $TlGaSe_2$.

$TlGaSe_2$ and $TlInS_2$ crystals are generally fabricated with Bridgman-Stockbarger method named after Harvard physicist Percy Williams Bridgman and MIT physicist Donald C. Stockbarger which is a popular method to produce certain semiconductors where Czochralski method is more difficult. Crystal lattice of $TlGaSe_2$. Anion layers consist of Se tetrahedron centered by Ga atoms. Tl ions depicted by dark circles are between the layers as shown in the figure [6].

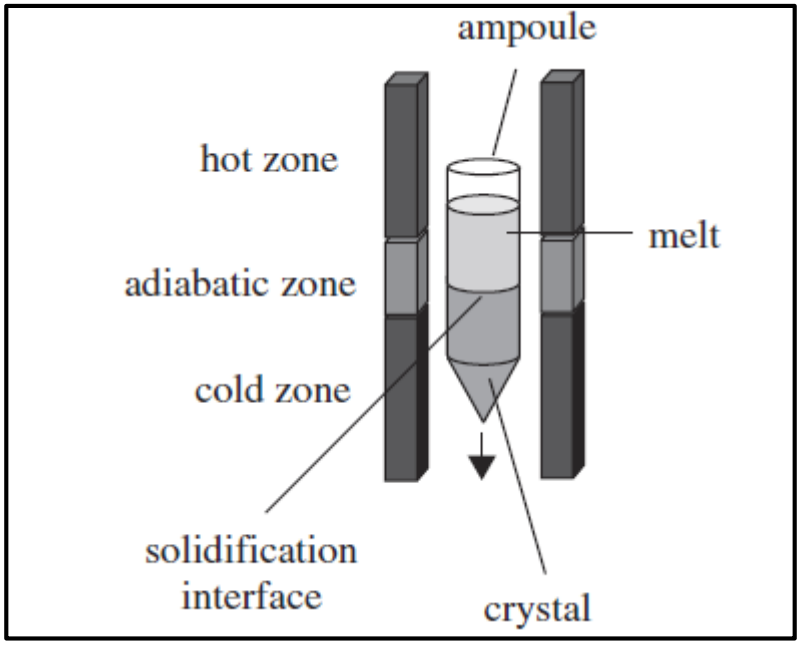

Figure 2.2: Bridgman method.

Melted polycrystalline materials inside the ampoule are cooled from the end of the seed crystal. The crucial part of this process is to tune up the cooling temperature and growth speed. The growth process works as shown in Figure 2.2 [7].

3. EXPERIMENTAL DETAILS

Undoped high-quality $TlGaSe_2$ and $TlInS_2$ samples were used in our experiments. Electric fields are applied with Tektronix DC Power Supply positioning the sample between two copper plate. X-Ray Diffraction and X-Ray Reflection experiments are conducted with Rigaku Smartlab X-ray diffractometer. (Cu-Kα radiation, $\lambda = 0.15418$nm) and Atomic Force Microscopy experiment are conducted with Nanoscope multimode AFM.

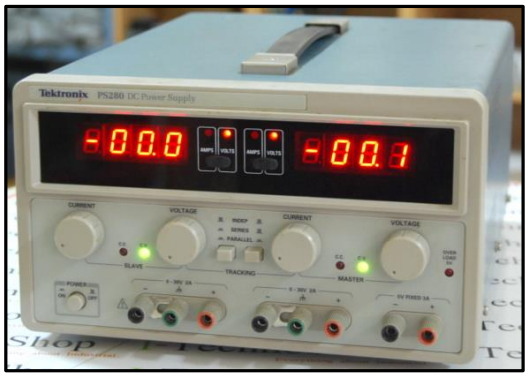

Figure 3.1: Tektronix PS 280 DC Power Supply.

Figure 3.2: Rigaku Smartlab X-ray diffractometer.

Figure 3.3: Nanoscope multimode AFM.

4. RESULTS AND THEORY

4.1. XRD Theory

Crystal structure can be examined with photon, neutron or electron diffraction. Diffraction depends on the wavelength and the crystal structure. As a result of the diffraction from every atom forming the crystal of an optical wave with a wavelength as far as 5000Å results with optical diffraction. If the incident radiations wavelength is near to the lattice parameter or smaller the diffraction can occur in very different directions.

Bragg's Law is a simple and elegant form of giving coherent and incoherent angles for scattering from a crystal lattice. When X-rays interfere with a surface they move electron clouds because of their electromagnetic wave nature resulting re-radiating waves in the same frequency. This phenomenon is called Rayleigh (elastic scattering) scattering [8-11]. A similar scattering occurs when an unpaired electron interacts with a neutron wave, nuclei or a coherent spin interaction. These constructive or destructive re-emitted wave fields produce a diffraction pattern on the intensity counting detector [12-13].

4.2. Bragg Interpretation of The Laue Condition

Any three lattice points which can form a triangle defines a plane called lattice plane. These lattice planes can be used to show a particularly simple interpretation of the diffraction from the lattice. Distance of these three lattice points from the origin must be an integer multiple of the basis vector as the basis vectors are the smallest vectors which can define next closest parallel plane. If we call these points which are the integer multiple of the basis vector as m,n, o then these points should be h' = 1/m k' = 1/n and l' = 1/o in reciprocal space. Thus h, k' and l' points will become (hkl) called Miller indices when multiplied by an integer *p*. Between these planes formed with h, k, l indices we can form other equivalent planes containing the same density of atom which their numbers are exactly *p* times of the original planes. We can now obtain index triplet (hkl) of co-prime integers using reciprocal values of points forming these equivalent planes.

Supposing the two vectors forming the lattice plane are $\frac{a1}{h'} - \frac{a2}{k'}$ and $\frac{a3}{l'} - \frac{a2}{k'}$ their vector product;

$$\left(\frac{a1}{h'} - \frac{a2}{k'}\right) x \left(\frac{a3}{l'} - \frac{a2}{k'}\right)$$
$$= -\frac{1}{h'k'}(a1\ x\ a2) - \frac{1}{k'l'}(a2\ x\ a3) - \frac{1}{h'l'}(a3\ x\ a1) \qquad (4.1)$$

is perpendicular to the plane (hkl). The multiplication of this vector by $2\pi\ \frac{h'k'l'}{[a1.(a2\ x\ a3)]}$
will give us;

$$G_{hkl} = 2\pi\ (h'\frac{a2\ x\ a3}{a1.(a2\ x\ a3)} + k'\frac{a3\ x\ a1}{a1.(a2\ x\ a3)} + l'\frac{a1\ x\ a2}{a1.(a2\ x\ a3)}) \qquad (4.2)$$

If we call the distance between parallel planes d_{hkl};

$$d'_{hkl} = \frac{a_1}{h'}\cos\alpha\ (a_1, G_{hkl}) = \frac{a_1}{h'}\frac{a_1 \cdot G_{hkl}}{a_1 G_{hkl}} = \frac{2\pi}{G_{hkl}}p \qquad (4.3)$$

Therefore, the distance to the nearest lattice plane is;

$$d_{hkl} = \frac{d'_{hkl}}{p} = \frac{2\pi}{G_{hkl}} \qquad (4.4)$$

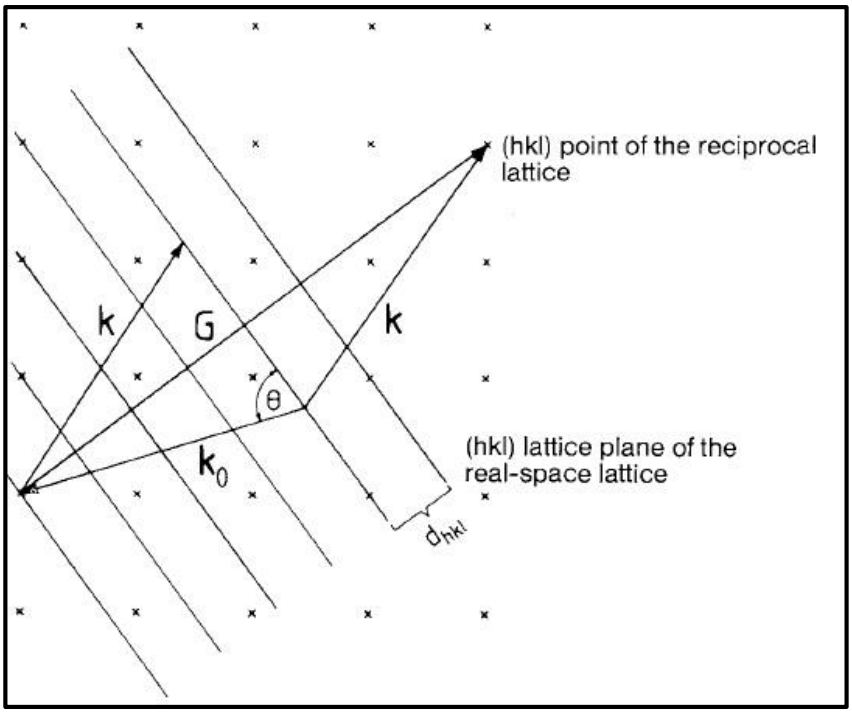

Figure 4.1: Bragg interpretation of constructive and destructive scattering conditions.

In this figure where real and reciprocal spaces are shown superposed we can obtain scattering conditions by taking modulus of the equation $G = K$

$$G_{hkl} = \frac{2\pi}{d_{hkl}} = 2k_0 \sin\ \theta \tag{4.5}$$

Which lead us to the Bragg equation.

$$\lambda = 2\mathrm{d} \sin\theta \tag{4.6}$$

Where d is the interplanar distance, λ is the wavelength of the incident beam comparable to atomic spacings (Bragg's condition). This equation indicates that waves behave as if they were reflected from the lattice planes. The Bragg reflection expression comes from this explanation [14]. To create a constructive interference the path difference between these so called reflected waves should be an integer multiple of the wavelength of the radiation. Thus, equation becomes:

$$n\lambda = 2\mathrm{d} \sin\theta \tag{4.7}$$

This expression is known as Bragg's law. Basically, it points out coherent and incoherent scattering angles from a crystal lattice. Which let us characterize material's structure deriving interplanar distance *d*.

4.3. XRD Results

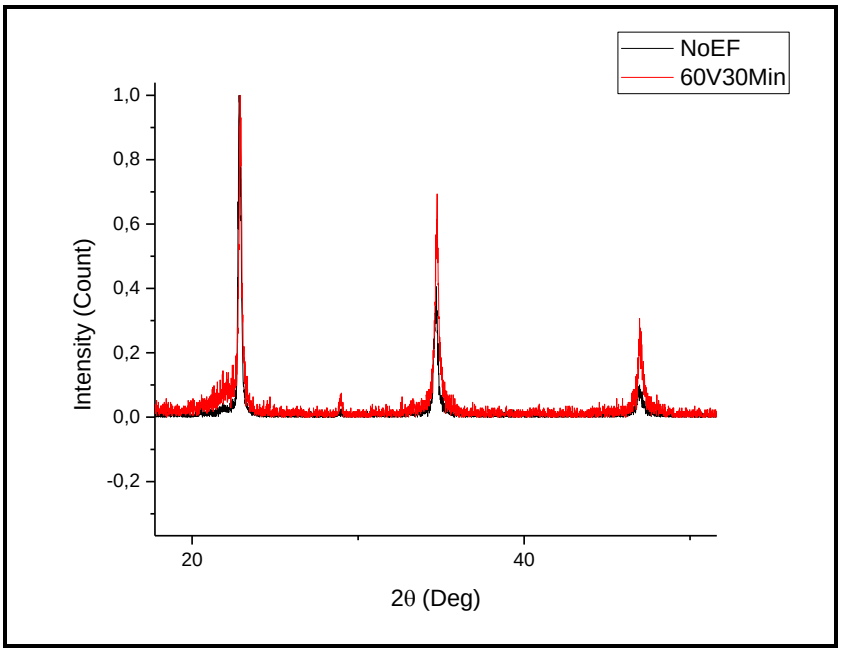

Figure 4.2: TlGaSe2 B Crystal under no electric field and under 60V.

This is an XRD result (Figure 4.2) of B crystal with no electric field applied and +60V applied for 30 minutes. We observed a small shifting of peaks. Which may indicate to a change in the crystal's structure.

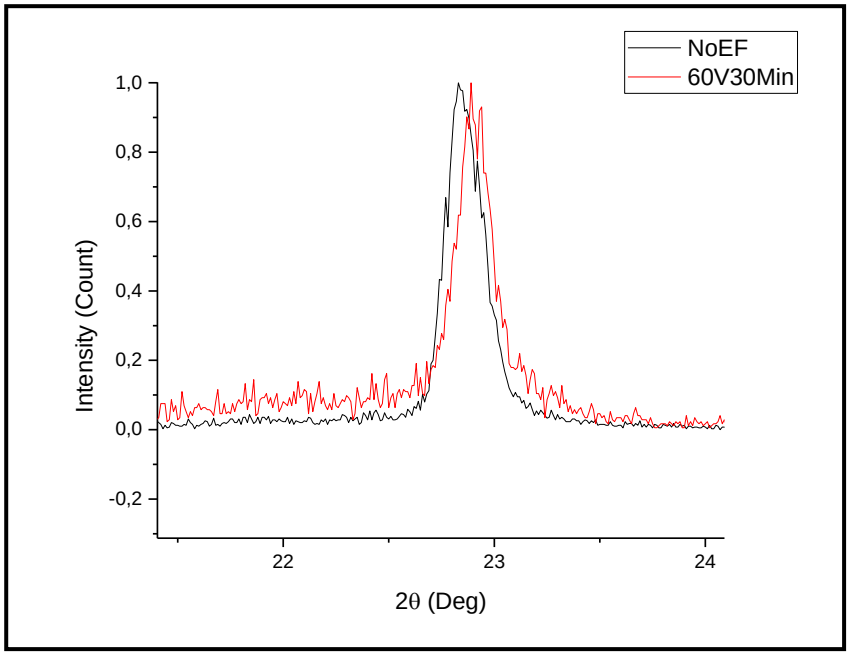

Figure 4.3: $TlGaSe_2$ B Crystal Shifting of first peak.

In this XRD graphic, we magnified the first peak of the previous graphic, to observe the shift in first peak explicitly. The difference $\Delta\theta \approx 0{,}06$ degree. As shown in Figure 4.3.

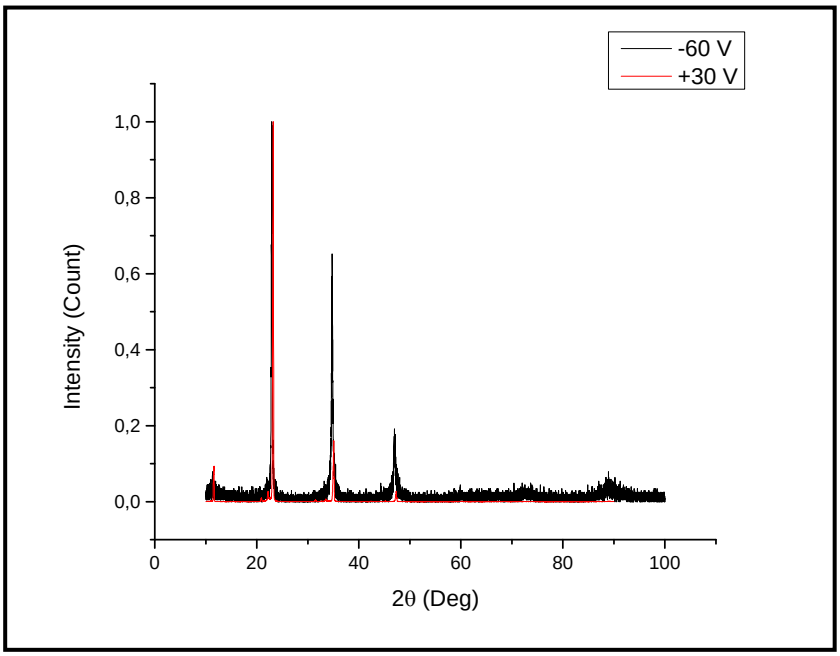

Figure 4.4: TlGaSe2 A Crystal under -60V and +30V.

In this experiment shown in Figure 4.4, We tryed to observe the effect of positive and negative electric field to see if the shifting in peaks will becomes larger. First -60V then +30V is applied to the crystal for 30 minutes.

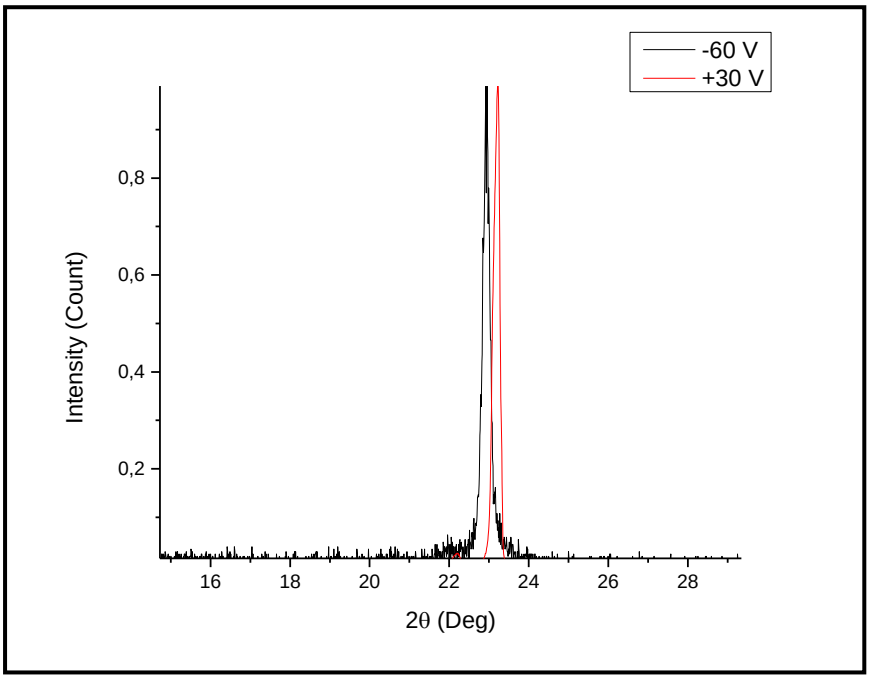

Figure 4.5: $TlGaSe_2$ A Crystal Shifting of first peak.

This is a magnified first peak of the A crystal's XRD results shown in Figure 4.5, where we can observe a change in first peak $\Delta\theta \approx 0.3$ Degree. This result removed the doubt on the structural change, and led us look for different crystals to find a bigger change.

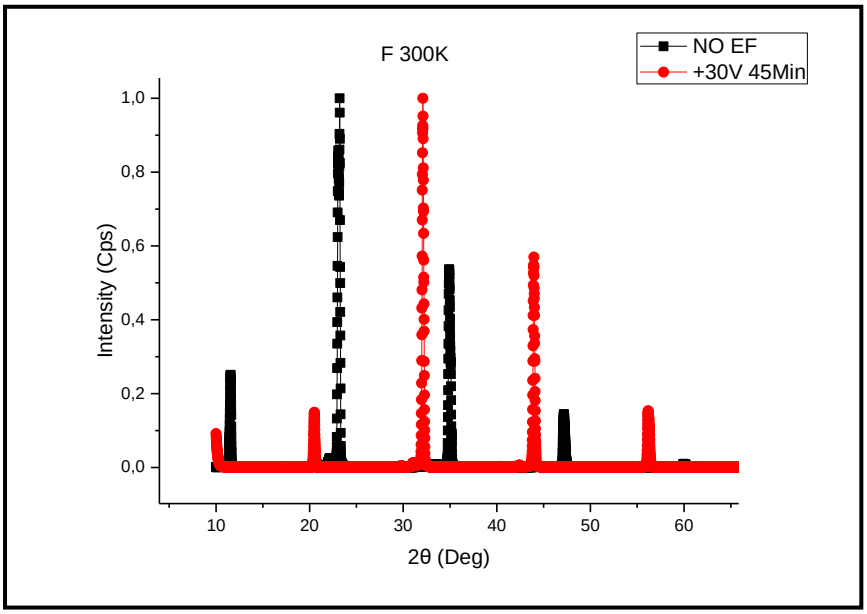

Figure 4.6: $TlGaSe_2$ F Crystal.

XRD image taken without electric field and after +30V applied for 45 minutes to the F crystal with higher quality than our other samples is shown in Figure 4.6. Results show that the shifting in peaks are as high as $\Delta\theta \approx 9$ degrees, which for a structrual change in XRD is immense.

Using Bragg's law one can find the change in d for second peak with highest intensity;

$$n\lambda = 2d \sin\theta \tag{4.8}$$

Using Cu target;

$$\lambda = 0{,}154\ nm \tag{4.9}$$

X-Ray sensor is at 2θ;

$$2\theta_0 \cong 23° \ and\ 2\theta_1 \cong 32° \tag{4.10}$$

$$d = \frac{n\lambda}{2\sin\theta} \tag{4.11}$$

Therefore,

$$d_0 = 0{,}772\ nm \tag{4.12}$$

$$d_1 = 0{,}558\ nm \tag{4.13}$$

$$\Delta d = 0{,}772 - 0{,}558 = 0{,}214\ nm \qquad (4.14$$

The change in *d* is 27,7%. This is a very big difference. There might be another reason to obtain such a shift in XRD plots which can be explained by the bending of the surface meaning the change in the surface normal according to *r*.

4.4. XRR Theory

X-Ray Reflectivity is a high precision non-destructive technique which can be used to determine film thickness, density and roughness. Thickness determination can be achieved between 2-200 nm with a precision of about 1-3 Å. As the incident angle is small, the penetration depth is small too which means this is a very surface sensitive technique. The principle underlying this method is to monitor the intensity of x-rays reflected by a sample at grazing angles. For incident angles below critical angle θ_c total external reflection occurs. Density of the film can be obtained with this critical angle θ_c. For the angles above θ_c film thickness and roughness is responsible for the intensity of reflected beam. There are many theories explaining why and how the reflection occurs between media interfaces starting with Fresnel Equations.

In our work, we used two different theories. First one is Porod's Law by Austrian physicist Günter Porod which describes the asymptote of the scattering intensity I (q) for large scattering wavenumbers. The second one is Guinier's Law by French physicist André Guinier which describes the scattering intensity *I(q)* for small wavenumbers.

4.4.1. Debye Equation

Debye equation is a direct way to give scattering intensity where coordinates of atoms inside the particle is known. Assuming there are n atoms with scattering lengths $f_i(q)$, we can also assume $f_i(q)$ is constant in the small angle region. Thus;

$$f_i(q) = f_i(0) = f_i \tag{4.15}$$

Now we can write an equation for the average intensity;

$$I(q) = \sum_{i=1}^{n}\sum_{j=1}^{n} f_i f_j \frac{\sin(qr_{ij})}{qr_{ij}} \tag{4.16}$$

Where $r_{ij} = |r_i - r_j|$ and the sum includes all the atoms in the particle.

This equation is derived by Debye in 1915 [15]. which we can obtain an exact formula for the small-angle scattering intensity. But it's not possible to solve the inverse problem due to the high number of terms generated by the double sum. However, it can be used to calculate scattering intensity from known shapes of particles. If a density distribution ρ(r) is used to define a particle instead of an atomic set, Debye equation becomes;

$$I(q) = \iint_V \rho(r_1)\,(r_2)\frac{\sin(qr_{12})}{qr_{12}} dr_1 dr_2 \tag{4.17}$$

Defining an auto-correlation expression;

$$\rho^2(r) \equiv \int\int\int dV_1 \rho(r_1)\rho(r_2) \tag{4.18}$$

We will obtain a new expression integrating it over the C-space;

$$I(q) = \int\int\int dV \rho^{-2}(r) e^{-iqr} \tag{4.19}$$

The reduced form can be written as;

$$I(q) = \int 4\pi r^2 \, dr \rho^{-2}(r) \frac{\sin qr}{qr} \tag{4.20}$$

This is the most appropriate form of the equation to apply in many cases.

4.4.2. Correlation Function

Supposing there is no correlation in between two points separated widely, at large r electron densities, ρ becomes independent and can be replaced with the mean value $\bar{\rho}$. The auto-correlation Equation 4.10 approach to a constant value; $V\bar{\rho}^2$ which doesn't contain any information. Therefore auto-correlation function should be redefined using electron density fluctuation ɳ instead of the electron density ρ.

$$\eta^{-2} = (\widetilde{\rho - \bar{\rho}})^2 = \bar{\rho}^2 - V\bar{\rho}^2 = V\gamma(r) \tag{4.21}$$

Comparing the Equation 4.10 and Equation 4.13 we can explain $\gamma(r)$ as the average of the product of two fluctuations at a distance r.

4.4.3. Scattering in the Born Approximation

If we assume that the material is homogenous at our measurement scale except for the surface. We can ignore the atomic surface. This is an acceptable approximation for small angle scattering where $qa \ll 1$ condition is satisfied, where q is the wavenumber ($4\pi \frac{\sin\theta}{\lambda}$), 2θ is the scattering angle, λ is the wavelength of the radiation and a is a length scale for inhomogeneity. Born approximation gives the differential cross section for scattering of the radiation by a system with the expression [16-17];

$$\frac{d\sigma}{d\Omega} = N^2 b^2 \int_V dr \int_V dr' e^{-iq(r-r')} \tag{4.22}$$

where, N is the number density of scattering particles and b is the Thompson scattering length of the electron.

$$b = \frac{e^2}{mc^2} \tag{4.23}$$

These integrals are over the volume of the solid and the wave number q is defined as the difference between incident and scattered wave vectors.

$$q \equiv k_2 - k_1 \tag{4.24}$$

Volume integrals in the equation 4.14 can be converted to surface integrals to obtain;

$$\frac{d\sigma}{d\Omega} = N^2 b^2 \frac{1}{(qA)^2} \int_S \int_S (dS.A)(dS'.A) e^{-iq.(r-r')} \tag{4.25}$$

Where A is an arbitrary unit vector in space and dS is the differential surface vector which is perpendicular to the surface. Considering we have a rough surface dS will be chosen as the *(x,y)* plane. If we chose the arbitrary vector A to be the unit vector $\hat{z}$ equation 4.17 can be rewritten as;

$$\frac{d\sigma}{d\Omega} = \frac{N^2 b^2}{q_z^2} \int \int_{S_0} dxdy \int \int_{S_0} dx'dy' \exp\{-iq_z[z(x,y) - z(x',y')]\} exp\{-i[q_x(x-x') + q_y(y-y')]\} \tag{4.26}$$

Where, S_0 is the surface of the *(x,y)* plane and *z(x,y)* is the height of the surface. Now we will assume that $[z(x,y) - z(x',y')]$ is a Gaussian random variable whose distribution is related to coordinates,

$$(X,Y) \equiv (x' - x, y' - y) \tag{4.27}$$

More specifically,

$$\langle [z(x,y) - z(x',y')]^2 \rangle = g(X,Y) \tag{4.28}$$

From the equation 4.17 we can write for an area $(L_x L_y)$ of the surface,

$$\frac{d\sigma}{d\Omega} = \frac{N^2 b^2}{q_z^2} L_x L_y \int \int_{S_0} dX dY \; e^{-q_z^2 g(X,Y)/2} \; e^{-i(q_x X + q_y Y)} \tag{4.29}$$

Now we can obtain direct expressions for $S(q)$ for different models of $g(R)$.

4.4.4. Porod's Law

Porod's Law is concerned with the intensity I (q) where the wavenumbers are smaller compared to Bragg diffraction but larger than Guinier's. Scattering vector q is smaller or near 1 nm^{-1}. Using Porod's Law we can't talk about our sample at atomic level but we can describe its electron density which will lead us to the shape of particles on the surface and their relations.

For a smooth surface where $g(X,Y) = g(R) = 0$ Equation 4.21 becomes;

$$S(q) \equiv \frac{d\sigma}{d\Omega} = \frac{1}{N^2 b^2 L_x L_y} = \frac{4\pi^2}{q_z^2} \delta(q_x)\delta(q_y) \tag{4.30}$$

The born approximation is valid under two conditions,

i) Where q is large enough so that the scattering is weak
ii) Where surfaces are locally clear-cut on a lenght scale $\leq 1/q$

At these length scales, average smooth surface can be defined. We can now derive $\bar{S}(q)$ by averaging results over all directions of q.

$$\bar{S}(q) = \frac{1}{4\pi} \int \int S(q) \sin\omega \, d\omega \, d\varphi \tag{4.31}$$

Where, ω and φ are polar angles of the q vector. For a constant magnitude of q,

$$\sin\omega \; d\omega \, d\varphi = \frac{dq_x dq_y}{q^2 \cos\omega} \tag{4.32}$$

Therefore, for a smooth surface equation 4.22 becomes,

$$\bar{S}(q) = \frac{2\pi}{q^4} \tag{4.33}$$

Therefore;

$$I\,(q) \;\cong\; Sq^{-4} \tag{4.34}$$

The standard form of Porod's Law indicates the intensity for a flat interface where S is the surface area of particles. The power q^{-4} is reproduced by the factor $1/\sin^4\theta$ in Fresnel Equations of Reflection [17].

4.4.5. Guinier's Law

Guinier's Law is concerned with the I (q) where the wavenumbers are much smaller compared to Bragg diffraction. By using the Guinier's Law we can obtain data about the radius of gyration of the scattering objects R_g.

Radius of gyration or gyradius is defined as,

$$R_g^2 = \frac{\int \rho(\mathbf{r})|\mathbf{r}|^2 dV}{\int \rho(\mathbf{r}) dV} \tag{4.35}$$

where ρ is the scattering length density at distance **r** from the center of the particle, R_g represents the effective size of the scattering particle.

The efficacy of the Guinier's Law is that R_g is independent of the absolute intensity $\mathrm{I}(0)$. Guinier approximation works well for all shapes of particles. If the shape of particle is known, then size of particles can be calculated by using the formula R_g^2. For a sphere of radius R; [18].

$$R_g = \sqrt{3/5}R \tag{4.36}$$

To examine the scattering intensity $I(s)$ at low angles we can substitute the Mclaurin series;

$$\frac{\sin qr}{qr} = 1 - \frac{q^2r^2}{6} + \frac{q^4r^4}{120} - \cdots \tag{4.37}$$

If we restrict the Mclaurin serie to the first two terms, then around $q = 0$;

$$I(q) = I(0)\left(1 - \frac{q^2R_g^2}{3}\right) * \tag{4.38}$$

where;

$$I(0) = 4\pi \int_0^D \gamma(r)r^2dr \tag{4.39}$$

and

$$R_g^2 = \frac{1}{2}\frac{\int_0^D \gamma(r)r^4dr}{\int_0^D \gamma(r)r^2dr} \tag{4.40}$$

The expression at the right-hand side of equation * can be accepted as the first two terms of the Mclaurin series of function $\exp(-\frac{q^2\,R_g^2}{3})$. Thus, the beginning of the scattering curve can be rewritten for a number of terms proportional to q^4 [19].

$$I(q) = I_0\, exp(-\frac{q^2R_g^2}{3}) \tag{4.41}$$

This is the Guinier equation derived by French physicist André Guinier [20-23] in 1937. We will be using it to find radius of gyration R_g which is directly related to the scattering particle's radius.

4.5. XRR Results

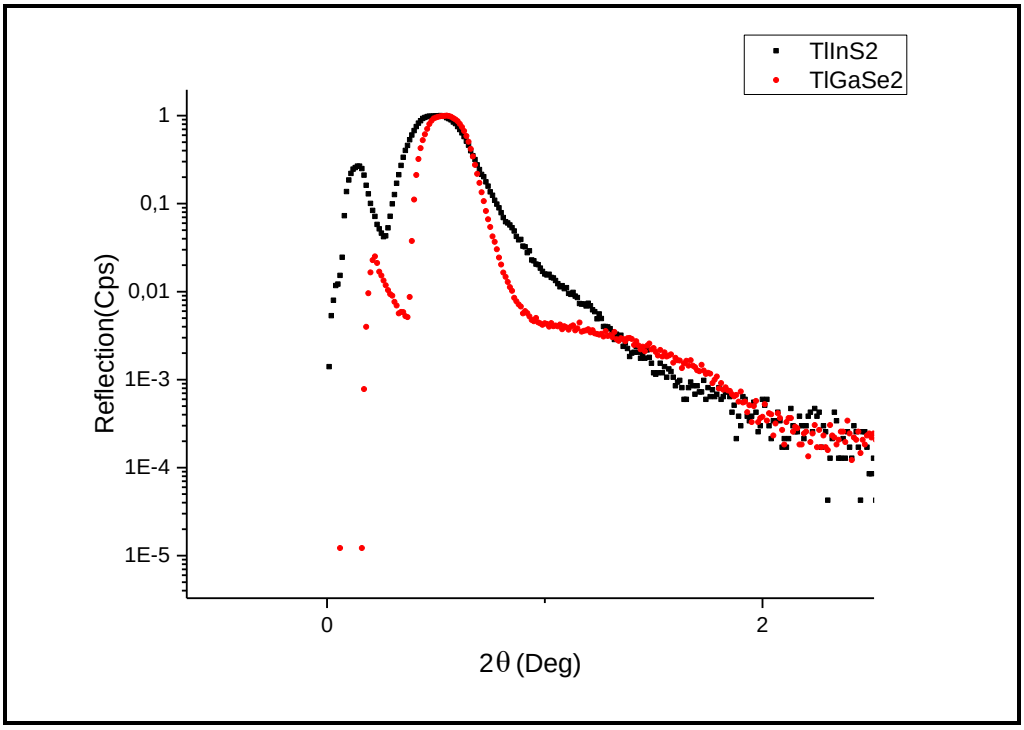

Figure 4.7: $TlInS_2$ and $TlGaSe_2$ Crystal.

This is an XRR plot of two different samples with different density. The shift in their critical angle shows explicitly there is a difference of density. Using general formula;

$$\theta_c = \sqrt{\frac{\rho N_a r_e \lambda^2 \sum_{i=1}^{N} c_i f_{1i}}{\pi \sum_{i=1}^{N} c_i M_i}} \tag{4.42}$$

where; ρ is the physical density(g/cm^3), Na is the Avogadro constant, M_i is molar mass (g/mol) and c_i is stoichiometric contribution with respect to the chemical formula of given compound.

Table 4.1: Used properties in density fit calculations. References for atomic scattering factors are given in text.

	f Atomic Scattering Factor (electrons)	**M Molar Mass (g/mol)**	**c Stoichiometry**
Tl	77.1952	204.37	1
Ga	29.7124	69.72	1
In	49.1374	114.82	1
Se	33.2061	78.96	2
S	16.3351	32.06	2

Table 4.2: Results of density calculations.

	θ_c **Critical Angle (°)**	**Density** gr/cm^3
$TlGaSe_2$	0.323	6.3079761
$TlInS_2$	0.308	5.7043758

We obtained results in Table 4.2; which are in a good agreement with known data. No oscillations observed; meaning either our sample's film thickness is too high or the surface is too rough. Atomic scattering form factors are taken from [24].

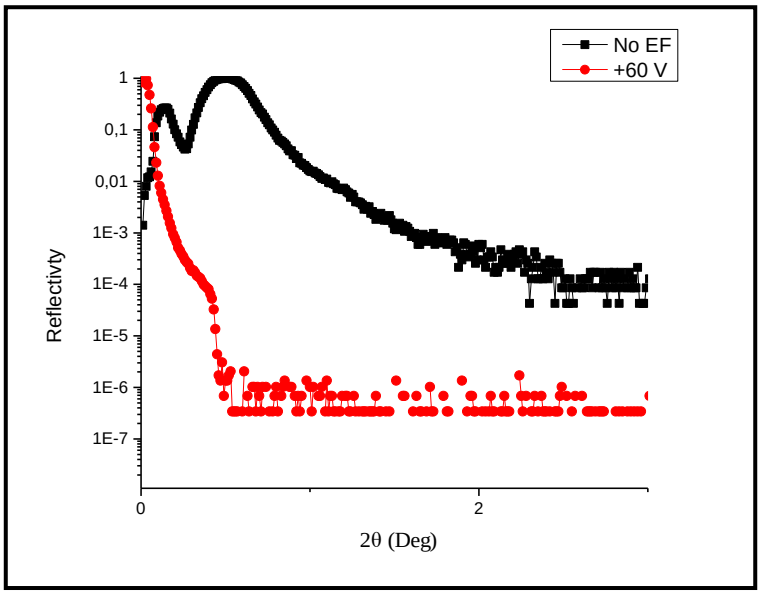

Figure 4.8: $TlInS_2$ Crystal.

After we studied structural properties, We wanted to investigate surface properties. In order to realize this study we have used XRR technique. This is the

XRR image of a $TlInS_2$ crystal under no electric field and +60V for 45 minutes shown in Figure 4.7. We determined that with the applied electric field there is a change in both reflection intensity and the critical angle, which refer to change in surface.

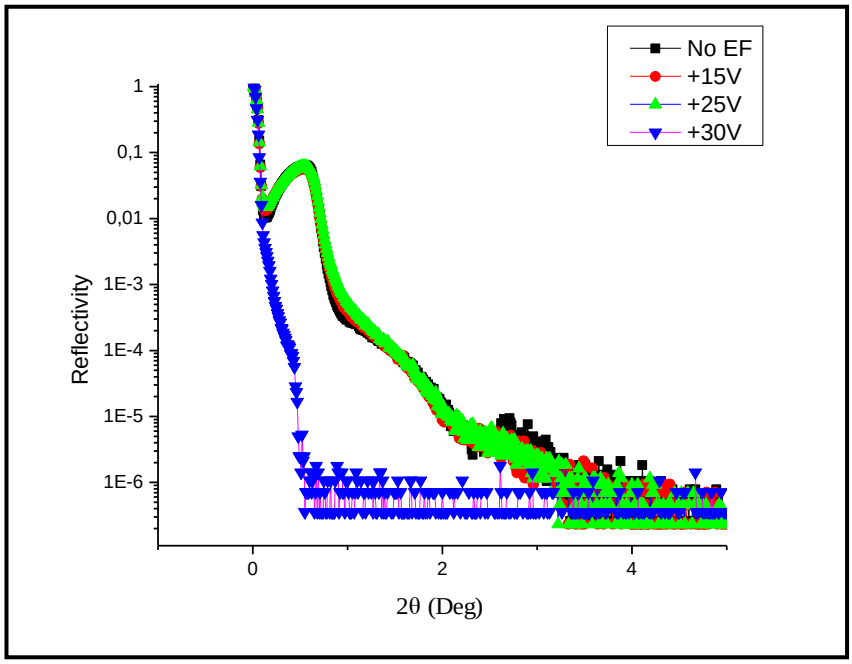

Figure 4.9: $TlGaSe_2$ B Crystal.

This is an XRR experiment with $TlGaSe_2$ crystal under no electric field and +15V, +25V, +30 V applied. This experiment indicated that the change in surface properties only occurs when the electric field is strong enough, which is +30V in this particular example shown in Figure 4.9.

This XRR experiment is conducted as a function of time in Figure 4.9. We wanted to observe both the rollback time of the scattering plot to its virgin condition and if it is an instant or gradual change. The result shows that the rollback time takes as far as 36 hours and no gradual change is observed.

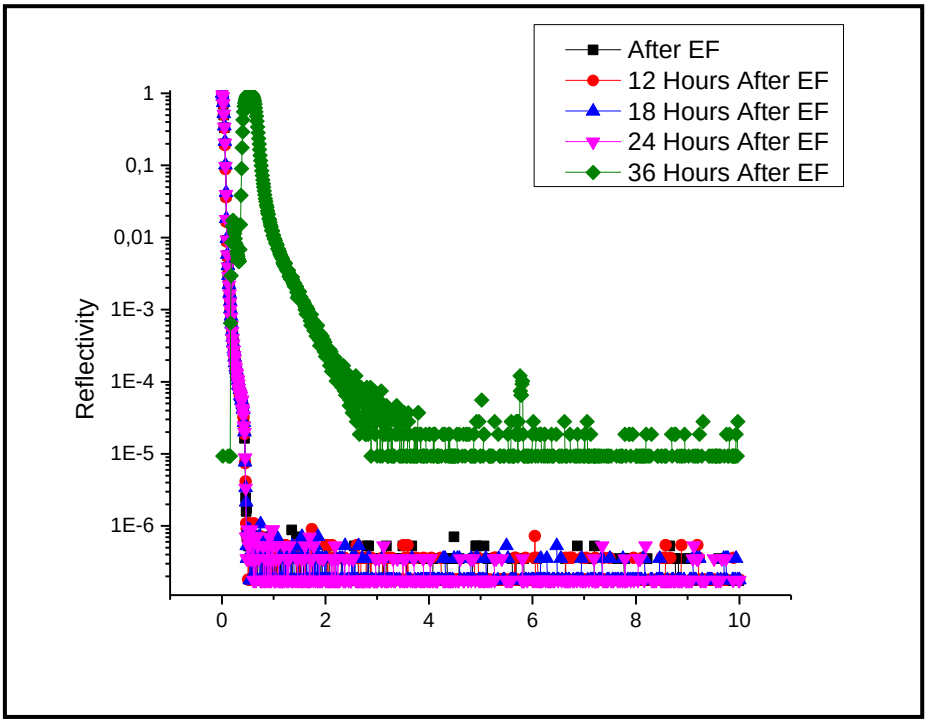

Figure 4.10: $TlGaSe_2$ B Crystal Reflectivity as a function of time.

This XRR experiment is conducted after an electric field of +60V applied for 30 min in Figure 4.10. Again at this experiment we observed a change in both reflection intensity and critical angle after applying an electric field.

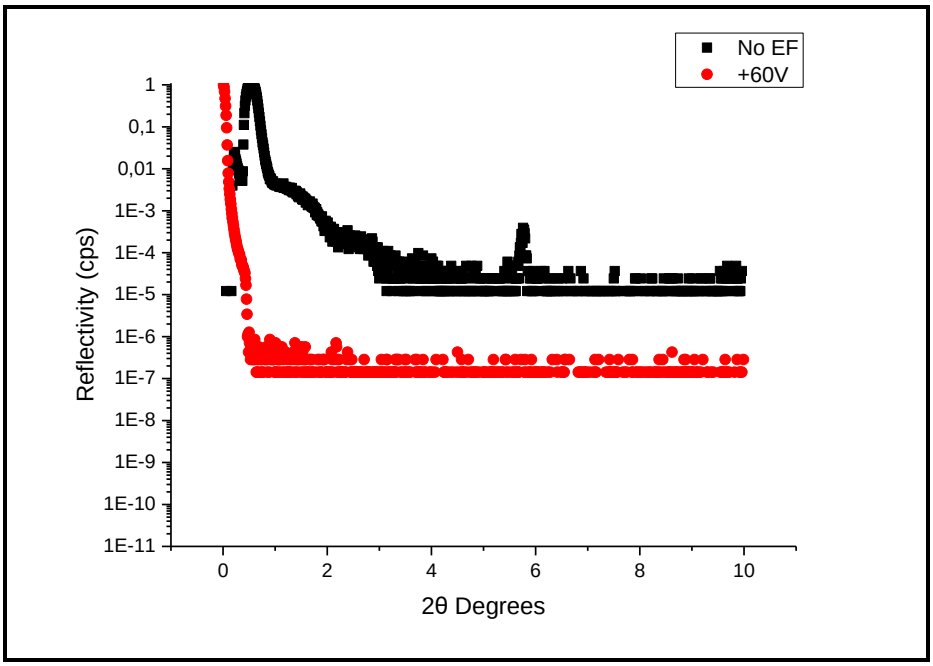

Figure 4.11: $TlGaSe_2$ B Crystal Reflectivity at No EF and 1+60V.

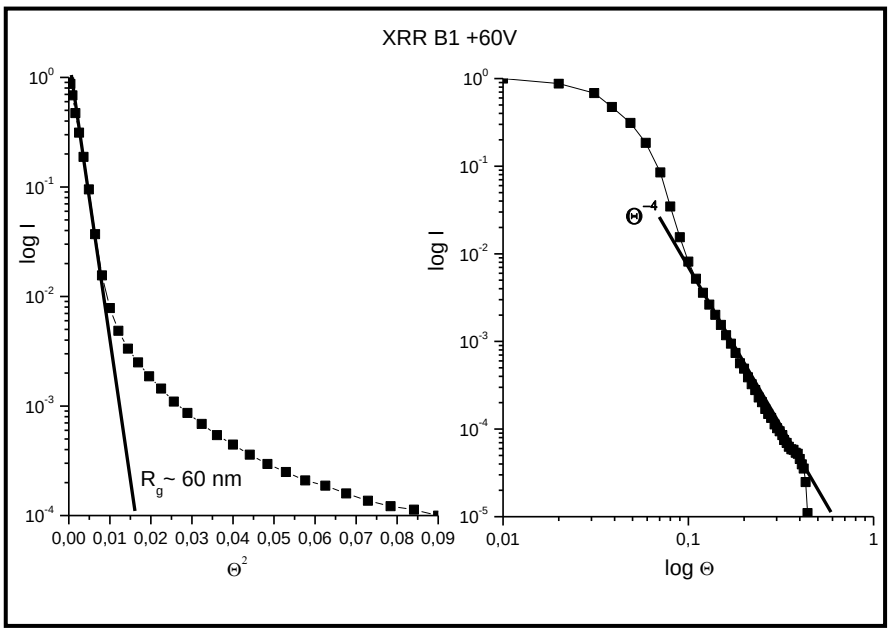

Figure 4.12: Guinier and Porod plots for $TlGaSe_2$ B1 Crystal.

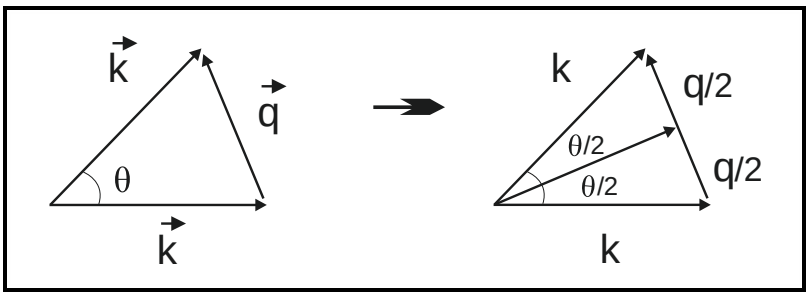

Figure 4.13: Construction of scattering vector.

We will now apply Guinier and Porod's theories to the data in Figure 4.10. As shown in Equation 4.16;

$$\vec{q} \equiv \vec{k}_2 - \vec{k}_1 \tag{4.43}$$

$$\sin\frac{\theta}{2} = \frac{q/2}{k} \tag{4.44}$$

$$q = 2k\sin\frac{\theta}{2} \approx \frac{2\pi}{\lambda}\theta \tag{4.45}$$

For Guinier theory as shown in Equation 4.32

$$I(q) \ = \ I_0 \ exp(-\frac{q^2 R_g^2}{3}) \tag{4.46}$$

If we take natural log of both side;

$$\log I \ = \ log \ I_0 - \frac{q^2 R_g^2}{3} \tag{4.47}$$

$$\log I \ = \ log \ I_0 - \frac{4\pi^2 R_g^2}{3\lambda^2} \theta^2 \tag{4.48}$$

We draw the fitting graphic $\log I - \theta^2$according these equations in Figure 4.11;

$$R_g \cong 60 \ nm \tag{4.49}$$

As shown in Equation 4.27;

$$R_g = \sqrt{3/5} R \tag{4.50}$$

Using Equation 4.40;

$$R \cong 46{,}475 \ nm \tag{4.51}$$

For Porod theory as shown in Equation 4.25;

$$I \ (q) \ \cong \ Sq^{-4} \tag{4.52}$$

If we take natural log of both side;

$$\log I = \log S - 4 \log q \tag{4.53}$$

$$\log I = (\log S - 4\log\frac{2\pi}{\lambda}) - 4\log\theta \tag{4.54}$$

According to taken fitting parameter, form Figure 4.12 (b) ,value of intercept, θ free term in Equation 4.54, is -6. If we substitute this value in mentioned, we take;

$$\log S - 4\log\frac{2\pi}{\lambda} \cong -6 \Rightarrow \log S = 4\log\frac{2\pi}{\lambda} - 6 \Rightarrow S = 10^{4\log\frac{2\pi}{\lambda}-6} = \left(\frac{2\pi}{\lambda}\right)^4 \cdot 10^{-6} \tag{4.55}$$

$$S \approx 2.77\ nm^2 \tag{4.56}$$

4.6. AFM

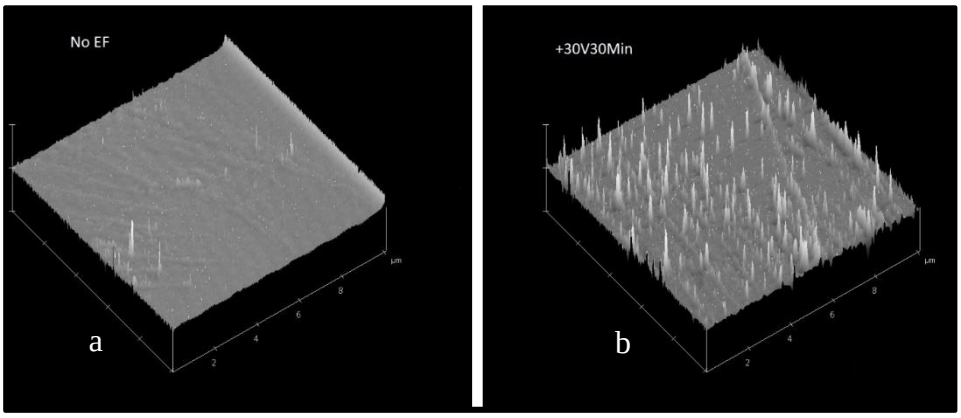

Figure 4.13: $TlGaSe_2$ B Crystal AFM Images. a) without electric field, b) after application +30V for 30 mins.

As observed in Figure 4.14 size of the island seen in AFM results are consistent with R_g.

Table 4.3: Digital Instruments NanoScope Device Specifications.

Scan size	10.00 μm
Scan rate	3.052 Hz
Number of samples	512
Image Data	Deflection
Data Scale	7 nm
X	2.000 μm/div
Z	7.000 nm/div

5. CONCLUSIONS

In this thesis, surface properties of $TlGaSe_2$ and $TlInS_2$ are investigated with X-Ray Diffraction, X-Ray Reflection and Atomic Force Microscopy techniques. The results show that, an externally applied electric field manipulates the surface structure according to Porod and Guinier theories which can be explained by the developpement of Volmer-Weber growth like islands.

- Externally applied electric field caused a shift of 0.1 degree for crystal B, 0.3 degree for crystal A and 9 degrees for crystal F in the XRD data, which can be explained by either a major change in *d* or change in the surface normal.
- Calculations showed that density data obtained with θ_c is in a good agreement with known $TlGaSe_2$ and $TlInS_2$ density.
- Externally applied electric field also caused a change in XRR data of both $TlGaSe_2$ crystal B and $TlInS_2$ crystal. Change observed only with applied electric fields larger than 30V.
- Porod fitting in scattering intensity proved the change on the surface caused by particles with surface S.
- Guinier fitting showed the approximate radius of gyration of the scattering objects after the electric field applied.
- XRR experiments as a function of time demonstrates that $TlGaSe_2$ crystal has a long-term memory up to 36 hours.
- AFM images proved the change on the surface structure and verified our Porod and Guinier approach.
- Results show beyond any doubt, under the effect of an applied positive voltage to the surface, negative charged entities are attracted at this direction.

REFERENCES

[1] Seyidov M. Y., Suleymanov R. A., Balaban, E., Şale Y., (2013), "Imprint Electric Field Controlled Electronic Transport in TlGaSe2 Crystals", Journal of Applied Physics, 114 (9), 093706.

[2] Babaev S., Mammadov T., Mikailov F., (2005), "Memory Efffect in Ferroelectrics with Layer Structure", Fizika-Riyaziyyat və Texnika Elmləri Seriyası, Fizika və Astronomiya, 2, 20-24.

[3] Seyidov M. Y., Suleymanov R., Balaban E., Şale Y. (2014), "Field Induced Rectification and Memristive Behavior of TlGaSe2 Layered Semiconductor", Applied Physics Letters, 105 (15), 152106.

[4] Seyidov M. Y., Suleymanov R. A., Şale Y., Balaban E., (2014), "Enhanced Excitonic Photoconductivity Due to Built-in Internal Electric Field in TlGaSe2 Layered Semiconductor", Journal of Applied Physics, 116 (21), 213702.

[5] Seyidov M. Y., Suleymanov R. A., Balaban E., Şale Y, (2014), "Enhancing the Photoresponse of a TlGaSe2 Semiconductor for Ultraviolet Detection Applications", Physica Scripta, 90 (1), 015805.

[6] Henkel W., Hochheimer H., Carlone C., Werner A., Ves S., Schnering H. v., (1982), "High-Pressure Raman study of the Ternary Chalcogenides $TlGaS_2$, $TlGaSe_2$, $TlInS_2$, and $TlInSe_2$", Physical Review B, 26 (6), 3211.

[7] Lalena J. N., Cleary D. A., Carpenter E., Dean N. F, (2008), "Inorganic Materials Synthesis and Fabrication" 1st Edition, John Wiley and Sons.

[8] Strutt J. W., (1871), "On the Light from the Sky, Its Polarization and Colour", The London, Edinburgh, and Dublin Philosophical Magazine and Journal of Science, 41 (271), 107-120.

[9] Rayleigh J. W. S. B., (1871), "On the Scattering of Light by Small Particles", Philosophical Magazine Series 4, 41 (275), 447-454.

[10] Rayleigh L., (1881), "On the Electromagnetic Theory of Light", The London, Edinburgh, and Dublin Philosophical Magazine and Journal of Science, 12 (73), 81-101.

[11] Rayleigh L., (1899), "On the Transmission of Light through an Atmosphere Containing Small Particles in Suspension, and on the Origin of the Blue of the Sky", The London, Edinburgh, and Dublin Philosophical Magazine and Journal of Science, 47 (287), 375-384.

[12] Bragg W. L., (1929), "The Diffraction of Short Electromagnetic Waves by a Crystal", Scientia, 23 (45), 153.

[13] Bragg W. H., Bragg W. L., (1913), “The Reflection of X-Rays by Crystals”, Proceedings of the Royal Society of London, Series A, Containing Papers of a Mathematical and Physical Character, 88 (605), 428-438.

[14] Harald I., Lüth H., (1996), “Solid-State Physics, An Introduction to Principles of Materials Science”, 1st Edition, Springer-Verlag.

[15] Debye P., (1909), Der Lichtdruck auf Kugeln von beliebigen Material, Annalen der Physik, 30, 57.

[16] Debye P., Bueche A., (1949), “Scattering by an Inhomogeneous Solid”, Journal of Applied Physics, 20 (6), 518-525.

[17] Sinha S., Sirota E. B., Garoff S., Stanley, H., (1988), “X-Ray and Neutron Scattering from Rough Surfaces”, Physical Review B, 38 (4), 2297.

[18] Seeck O. H., Murphy B., (2015), “X-Ray Diffraction: Modern Experimental Techniques”, 1st Edition, Pan Stanford.

[19] Feigin L., Svergun D. I., Taylor G. W., (1987) “Structure Analysis by Small-Angle X-Ray and Neutron Scattering”, 1st Edition, Springer.

[20] Guinier A., (1939), “La Diffraction des Rayons X aux Tres Petits Angles: Applications a l'Etude de Phenomenes Ultramicroscopiques”, Annales de Physique, 12, 161-237.

[21] Guiner A., Fournet G.,Walker C., (1955), “Small Angle Scattering of X-Rays”, 1st Edition, John Wiley and Sons, New York.

[22] Guinier A., (1994), “X-Ray Diffraction in Crystals, Imperfect Crystals, and Amorphous Bodies”, 1st Edition, Courier Corporation.

[23] Pilz I., Glatter O., Kratky O., (1978), “Small-Angle X-Ray Scattering”, Methods in Enzymology, 61, 148-249.

[24] Web 1, (2017), http://henke.lbl.gov/optical_constants/asf.html, (Erişim: 07/02/2017).

BIOGRAPHY

Emir Suad OLCAY received his Bachelor of Science degree in Physics at Gebze Institute of Technology (2014). Continued his work as a graduate student in Gebze Technical University Graduate School of Natural and Applied Sciences under the consultancy of Prof.Dr. Rauf Suleymanlı between 2014-2017.

Currently teaching physics in private Private French High-School Saint-Joseph Istanbul and willing to continue working with Prof. MirHasan Seyitsoy and Prof. Rauf Suleymanli during his PhD program.